J. Electrochem. Sci. Eng. **13(5)** (2023) 753-770; http://dx.doi.org/10.5599/jese.1659

Open Access : : ISSN 1847-9286
www.jESE-online.org

Original scientific paper

Elucidating mechanistic background of the origin and rates of peroxide formation in low temperature proton exchange fuel cells

Ambrož Kregar[1,2,✉] and Tomaž Katrašnik[1]

[1]*University of Ljubljana, Faculty of Mechanical Engineering, Aškerčeva cesta 6, Ljubljana, 1000, Slovenia*

[2]*University of Ljubljana, Faculty of Education, Kardeljeva ploščad 16, Ljubljana, 1000, Slovenia*

Corresponding author: ✉ *ambroz.kregar@fs.uni-lj.si; Tel.: +386-1-4771-512*

Received: January 6, 2023; Accepted: July 3, 2023; Published: July 19, 2023

Abstract

Degradation of electrode-membrane assembly of the low-temperature hydrogen fuel cells represents one of the main obstacles in wider adoption of these clean and efficient electrochemical sources of electrical energy. Chemical degradation of proton exchange membrane is initiated by hydrogen peroxide formation, which forms in the fuel cell as a by-product to water in oxygen reduction reaction and decomposes to reactive radical species, damaging to the membrane chemical structure. Depending on the operating conditions of the fuel cell, the source of hydrogen peroxide can be either cathode, anode, or, as we argue in the paper, also the Pt particles in the membrane, which originate from the cathode catalyst dissolution, diffusion into the membrane and redeposition of Pt ions inside the membrane. In the paper we propose a mathematical model of intertwined physical processes in membrane and catalyst layer, aimed at unifying the description of hydrogen peroxide formation throughout entire membrane-electrode assembly at any fuel cell operating conditions. The model results, compared to experimental data, indicate that Pt particles inside the membrane can indeed be an important source of hydrogen peroxide in aged fuel cells. For a fresh fuel cell, numerical simulation using proposed model show that hydrogen peroxide can be formed at either cathode or anode, depending on the fuel cell operating condition, but with anode production being more prominent in standard fuel cell operating conditions.

Keywords

Fuel cell; membrane; degradation; hydrogen peroxide; modelling

Introduction

The use of hydrogen-fueled low-temperature fuel cells with proton-exchange membrane (LT-PEMFC) represent an important step in fulfilling the future goals of decarbonization of transport and energy sector. Electricity is produced in the fuel cell by oxidation of hydrogen fuel in anode catalyst layer, resulting in protons which travel through proton-conducting polymer membrane to

the cathode catalyst layer, where they are recombined with oxygen in reduction reaction. The resulting electric potential between anode and cathode can be used to extract useful work. Since the reactants are supplied to the membrane-electrode assembly (MEA) from external tanks, the size scaling of LT-PEMFC is much better compared to batteries, which makes the fuel cells especially suitable for a heavy-duty transport applications, such as trucks and buses [1].

Despite these clear advantages, LT-PEMFCs still suffer from several drawbacks. Among the most important ones is limited durability, caused by several degradation mechanisms of fuel cell components [2]. LT-PEMFC catalyst layer is typically composed of nanoscopic Pt particles, dispersed on a highly porous carbon matrix to provide both high specific surface area for electrochemical reactions and good diffusion properties for transport of reactants and products. Electrochemical oxygen reduction in the cathode catalyst results in high local electric potential, which, combined with relatively high temperatures of about 80 °C can lead to oxidation and corrosion of both Pt particles and carbon support, resulting in eventual loss of electrochemically active surface area [3-5]. Proton-exchange membrane, usually made from perfluorinated polymer materials such as Nafion, is also prone to degradation [6]. Most notably, the hydrogen peroxide, formed as a byproduct of oxygen-reduction reaction (ORR), can decompose in the presence of various metal ions into highly reactive radical species, which split chemical bonds in the membrane structure and result in loss of its proton conductivity and mechanical integrity [6,7].

While the basic electrochemical process of hydrogen peroxide formation is well understood [8], the specifics of its formation in fuel cell MEA are still a topic of debate. Since oxygen is one of the reactants in peroxide formation, the oxygen-rich cathode catalyst layer seems an obvious location of its origin. However, since hydrogen peroxide only forms when local electric potential between catalyst and adjacent ionomer (relative to RHE throughout the text) falls below 0.67 V compared to water, which is produced below 1.23 V [9], which is rarely encountered in cathode catalyst during normal fuel cell operation, the cathode peroxide formation might not be the main origin. Anode catalyst layer, on the other hand, features low electric potential ($\gtrsim$ 0 V), but low concentration of oxygen, which can only arrive to the anode by means of diffusion through the membrane, limits the rate of peroxide production in anode catalyst layer.

The third option is a formation of hydrogen peroxide inside the membrane [10]. In this case, the formation takes place on the surface of Pt particles, formed in the membrane due to catalyst layer degradation. Pt ions, resulting from dissolution of Pt particles in cathode catalyst layer, diffuse into the membrane where they are reduced to crystallite Pt particles, so-called Pt band, when encountering the hydrogen, which slowly diffuses from anode catalyst layer towards the cathode [11]. Raman spectroscopy measurements [12,13] of membrane chemical composition profile, published by Ohma *et al.* [10], show significant membrane degradation at the location of Pt band, which strongly indicates the formation of hydrogen peroxide inside the membrane and calls for better understanding of its relation to the formation rates in cathode and anode catalyst layer. We argue in this paper that Pt band particles in the membrane can feature appropriate electric potential to support the formation of hydrogen peroxide from the diffusive oxygen and protons, abundant inside the membrane.

Since *in situ* measurements of spatial distribution of hydrogen peroxide concentration throughout MEA are missing, it is difficult to conclude with high certainty which of the described peroxide formation processes is the most important. Experimental measurements show a strong dependence of formation rate on fuel cell operating conditions, such as fuel cell voltage, temperature and humidity [9]. These effects are well described by several existing models of peroxide formation. The first mathematical model was proposed by Sethuraman *et al.* [14], describing the peroxide

formation in both anode and cathode catalyst layer using Tafel equation describing the effects of voltage, temperature and humidity. The model was further developed by Chen and Fuller, which added a description of hydrogen peroxide decomposition in Fenton reaction [15], and in several papers by Wong *et al.* [16-18], in which they include the description of peroxide transport through the membrane, its decomposition in Fenton reaction and consequent chemical degradation. The model by Futter [19] is further expanded by adding the effects of pressure on peroxide formation rate.

Aforementioned models describe the rate of peroxide production in cathode and anode catalyst layer in various fuel cell operation conditions with good precision, but, to our best knowledge, no attempts have thus far been made to model the hydrogen peroxide formation on Pt band particles inside the membrane. The aim of this paper is therefore to propose a unified mathematical description of diffusion processes and electrochemical reactions involved in hydrogen peroxide production for all three components of MEA: cathode, membrane, and anode. This is achieved by combining the existing models of hydrogen peroxide formation, applicable in anode and cathode catalyst layer [15] and applying them to the Pt band particles inside the membrane [11]. The model thus allows direct comparison between peroxide formation rates in all there MEA components and enables elucidating causal relations of peroxide formation phenomena and comparison of formation rates at different locations at different fuel cell operating conditions.

Experimental

Modelling procedure

The proposed model considers three species involved in electrochemical hydrogen peroxide formation: hydrogen (H_2) and oxygen (O_2) as reactants and hydrogen peroxide (H_2O_2) as a product. To consistently describe electrochemical reactions in all three relevant sections of MEA. Cathode and anode layer are composed of a mixture of ionomer, highly porous carbon support on which Pt nanoparticles are dispersed, and void space allowing the diffusion of gases. Membrane is composed of ionomer in which electrically insulated Pt band particles can reside, providing electrochemically active surface area. Each of three modelled species (H_2, O_2 and H_2O_2) is described by a single one-dimensional concentration field in direction perpendicular to the MEA plane (x), describing the species concentration in the ionomer. The species concentration profiles are governed by a unified set of partial differential equations which apply throughout the entire modelling domain (cathode, membrane, and anode):

$$\left(\frac{\partial c_{H_2}(x,t)}{\partial t}\right)=\left(\frac{\partial c_{H_2}(x,t)}{\partial t}\right)_{dif}+\left(\frac{\partial c_{H_2}(x,t)}{\partial t}\right)_{EC} \quad (1)$$

$$\left(\frac{\partial c_{O_2}(x,t)}{\partial t}\right)=\left(\frac{\partial c_{O_2}(x,t)}{\partial t}\right)_{dif}+\left(\frac{\partial c_{O_2}(x,t)}{\partial t}\right)_{EC} \quad (2)$$

$$\left(\frac{\partial c_{H_2O_2}(x,t)}{\partial t}\right)=\left(\frac{\partial c_{H_2O_2}(x,t)}{\partial t}\right)_{dif}+\left(\frac{\partial c_{H_2O_2}(x,t)}{\partial t}\right)_{EC}+\left(\frac{\partial c_{H_2O_2}(x,t)}{\partial t}\right)_{fent} \quad (3)$$

describing three contributions to the dynamics: diffusion (dif), electrochemical reactions (EC) and Fenton reaction (fent). Each of the terms will be described in detail in the following sections.

Additionally, the model describes the local electric potential difference between Pt catalyst particle surface and adjacent ionomer (electric double layer potential) $U_{Pt}(x,t)$:

$$\left(\frac{\partial U_{Pt}(x,t)}{\partial t}\right)=\left(\frac{\partial U_{Pt}(x,t)}{\partial t}\right)_{EC}+\left(\frac{\partial U_{Pt}(x,t)}{\partial t}\right)_{cond} \tag{4}$$

governed by electrochemical reactions and electron conduction (cond) through catalyst support structure. As for the treatment of chemical species, Eqs. (1)-(3), the same set of equations is applied throughout the entire modelling domain, with the rates of processes determined by specific spatially dependent properties of the domain.

The processes described by the model are schematically presented in Figure 1. Note that the size and volumetric density of Pt particles in the membrane is not calculated by the model but taken as fixed initial condition.

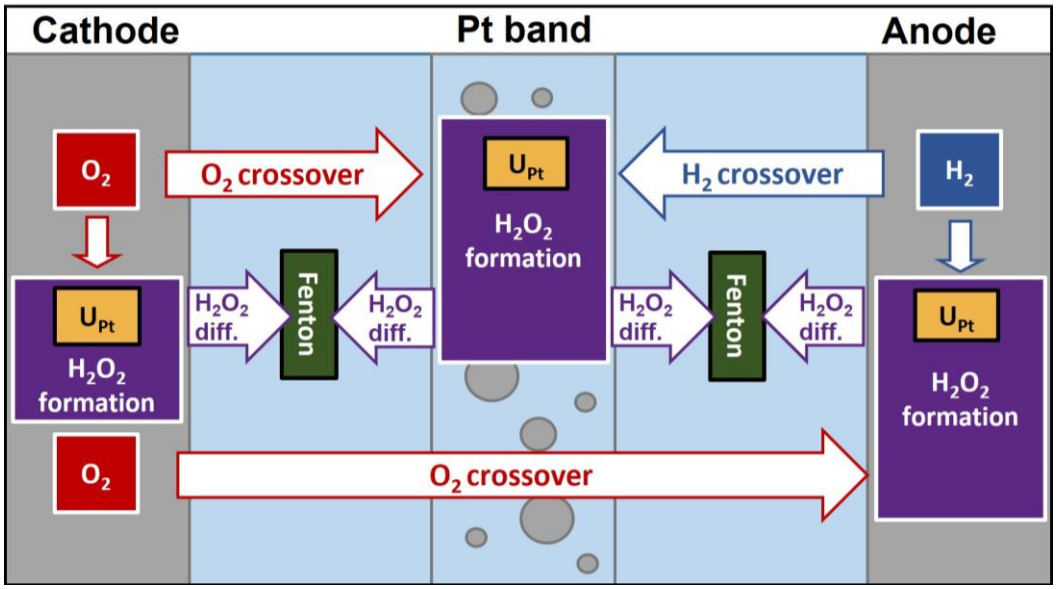

Figure 1. *Schematic representation of modelled processes: concentrations of hydrogen, oxygen and hydrogen peroxide are governed by diffusion, Fenton reaction, and electrochemical reactions between species, with rates determined by local electric potential* U_{Pt}

Diffusion model

Diffusion of species inside the membrane can be described by a diffusion equation with diffusion constant for each species $D_i = D_{i,ion}$, with i = H_2, O_2, H_2O_2. The description of diffusion process in anode and cathode is more challenging since the model needs to consider that species can diffuse through both ionomer (described by volume fraction ε_{ion}) and void space (ε_0) of the porous material. To address this challenge, we propose a diffusion equation with spatially dependent effective diffusion constant $\tilde{D}_i(x)$, describing parallel diffusion through both materials. To derive the mathematical expression $\tilde{D}_i(x)$, we first describe separately the species diffusion through each material. The molar flux through ionomer is described as

$$j_{i,ion}(x,t)=-D_{i,ion}\frac{\partial c_{i,ion}(x,t)}{\partial \tilde{x}}=-\frac{D_{i,ion}}{\tau_{ion}(x)}\frac{\partial c_{i,ion}(x,t)}{\partial x} \tag{5}$$

where we consider the fact that the actual path through the ionomer $\tilde{x}$ is longer than geometric path x by tortuosity factor τ_{ion}: $\tilde{x} = \tau_{ion}(x)\, x$. Similar expression is used for void fraction equation with diffusion constants $D_{i,0}$:

$$j_{i,0}(x,t) = -D_{i,0}\frac{\partial c_{i,0}(x,t)}{\partial \tilde{x}} = -\frac{D_{i,0}}{\tau_0(x)}\frac{H_i}{RT}\frac{\partial c_{i,0}(x,t)}{\partial x} \quad (6)$$

Here we assume that species concentration in ionomer c_{ion} and in void c_0 are always in equilibrium, determined by ionomer Henry constant H: $c_0=H/RT\ c_{ion}$ [17], which is reasonable considering that the ionomer film in catalyst layer is thin.

Total flux per geometric area is obtained by summation of ionomer and void flux, weighted by their volumetric ratio:

$$j_i(x,t) = \epsilon_{ion}(x)\,j_{i,ion}(x,t) + \epsilon_0(x)\,j_{i,0}(x,t) = -\tilde{D}_i(x)\frac{\partial c_{i,ion}(x,t)}{\partial x} \quad (7)$$

with resulting effective diffusivity

$$\tilde{D}_i(x) = \frac{\epsilon_{ion}(x)}{\tau_{ion}(x)}D_{i,ion} + \frac{\epsilon_0(x)}{\tau_0(x)}\frac{H_i}{RT}D_{i,0} \quad (8)$$

which is similar to Bruggeman expression $D_{eff} = D\varepsilon/\tau$. Different relations between tortuosity and porosity are proposed in the literature [20], in our model we choose a simple relation $\tau = \varepsilon^{1-\alpha}$ with $\alpha = 1.5$.

To determine the rate of concentration change in ionomer we again take into account that species accommodate prescribed volume in void and ionomer and that both concentrations are in equilibrium:

$$\left(\frac{\partial c_i(x,t)}{\partial t}\right)_{dif} = \frac{1}{\left(\epsilon_{ion}(x) + \epsilon_0(x)\frac{H_i}{RT}\right)}\frac{\partial}{\partial x}\left(\tilde{D}_i(x)\frac{\partial c_i(x,t)}{\partial x}\right) \quad (9)$$

In Eq. (9) we write $c_i(x,t) = c_{i,ion}(x,t)$ as all the concentrations in the reminder of the paper will refer to the concentration in ionomer phase. The same equation can be used to describe the transport of all three species i = H_2, O_2, H_2O_2 using their respective effective diffusion coefficient. The difference in transport properties between cathode, membrane, and anode are described by spatial distribution of ionomer $\varepsilon_{ion}(x)$ and void volume fraction $\varepsilon_0(x)$.

Electrochemical reactions

Hydrogen, oxygen, and hydrogen peroxide are all involved in electrochemical reactions on Pt surface in cathode and anode catalyst layer, where the rates are determined by electric potential of the Pt/C matrix. However, the reactions can also take place on the surface of Pt particles in so-called Pt band inside the membrane, which are electrically isolated from the catalyst layers [11]. The reactions in Pt band follow the same principles as in the catalyst layer, but their rate needs to be determined by the local electric potential on Pt particles, determined in turn by the rates of electrochemical reactions on their surface [11], which will be described in the next section.

In the model, we consider 4 electrochemical reactions [17]. If potential difference between catalyst and ionomer is larger than 0 V, the hydrogen reacts hydrogen oxidation reaction (HOR), producing protons [17]:

$H_2 \leftrightarrow 2H^+ + 2e^-$, $U_{HOR} = 0$ V (10)

This reaction is most prominent in the anode where hydrogen concentration is high. Note that since electrons are deposited on catalyst, the reaction tends towards lowering the potential of the catalyst on which it takes place.

Oxygen is reduced on the catalyst surface in two similar reactions. 4-electron oxygen reduction reaction (ORR4) results in water [17]:

$$O_2 + 4H^+ + 4e^- \leftrightarrow 2H_2O,\ U_{ORR4} = 1.23\ V \tag{11}$$

and takes place when electric potential is lower than 1.23 V. 2-electron oxygen reduction reaction (ORR2) is similar, but results in hydrogen peroxide formation [17]:

$$O_2 + 2H^+ + 2e^- \leftrightarrow H_2O,\ U_{ORR2} = 0.67\ V \tag{12}$$

and occurs only when electric potential is lower than 0.67 V. Since both reactions consume electrons and thus increase the electric potential on the catalyst, the resulting potential is typically closer to 1.23 V then 0.67 V, suppressing the formation of hydrogen peroxide.

Hydrogen peroxide can further react in peroxide reduction reaction (PRR) [17]:

$$H_2O_2 + 2H^+ + 2e^- \leftrightarrow 2H_2O,\ U_{PRR} = 1.67\ V \tag{13}$$

which takes place when electric potential is lower than 1.67 V.

The rates of electrochemical reactions, listed above, are calculated using modified Butler-Volmer equations which take into account concentrations and electric potential on the Pt particles, while they, in addition, consider also the diffusion limitations to species fluxes from bulk ionomer to the particle surface [11]. The equations for calculating the rates in [mol m^{-2} s^{-1}] are [11,17]:

$$j_{HOR}(x,t) = \frac{k_{HOR}\left(a_{H_2}(x,t)\,e^{\frac{2\alpha_{HOR}\left(U_{Pt}(x,t)-U_{HOR}\right)}{b_T}} - a_{H^+}\,e^{\frac{-2(1-\alpha_{HOR})\left(U_{Pt}(x,t)-U_{HOR}\right)}{b_T}}\right)}{1+k_{HOR}\dfrac{r_{Pt}(x)}{D_{H_2}c_{ref}}\,e^{\frac{2\alpha_{HOR}\left(U_{Pt}(x,t)-U_{HOR}\right)}{b_T}}} \tag{14}$$

$$j_{ORR4}(x,t) = \frac{k_{ORR4}\left(a_{O_2}(x,t)\,e^{\frac{-4(1-\alpha_{ORR4})\left(U_{Pt}(x,t)-U_{ORR4}\right)}{b_T}} - a_{H_2O}\,e^{\frac{4\alpha_{ORR4}\left(U_{Pt}(x,t)-U_{ORR4}\right)}{b_T}}\right)}{1+k_{ORR4}\dfrac{r_{Pt}(x)}{D_{O_2}c_{ref}}\,e^{\frac{4\alpha_{ORR4}\left(U_{Pt}(x,t)-U_{ORR4}\right)}{b_T}}} \tag{15}$$

$$j_{ORR2}(x,t) = \frac{k_{ORR2}a_{O_2}(x,t)\,e^{\frac{-2(1-\alpha_{ORR2})\left(U_{Pt}(x,t)-U_{ORR2}\right)}{b_T}}}{1+k_{ORR2}\dfrac{r_{Pt}(x)}{D_{O_2}c_{ref}}\,e^{-\frac{2(1-\alpha_{ORR2})\left(U_{Pt}(x,t)-U_{ORR2}\right)}{b_T}}} \tag{16}$$

$$j_{PRR}(x,t) = \frac{k_{PRR}a_{H_2O_2}(x,t)\sinh\dfrac{2\alpha_{PRR}\left(U_{Pt}(x,t)-U_{PRR}\right)}{b_T}}{1+k_{PRR}\dfrac{r_{Pt}(x)}{D_{H_2O_2}c_{ref}}\sinh\dfrac{2\alpha_{PRR}\left(U_{Pt}(x,t)-U_{PRR}\right)}{b_T}} \tag{17}$$

The rates of reactions j_r (r = HOR, ORR4, ORR2, PRR) are proportional to the reaction rate constants k_r. Species activities are calculated by dividing position- and time-dependent concentrations with the reference values: $a_{H_2}(x,t) = c_{H_2}(x,t)/c_{ref}$, $a_{O_2}(x,t) = c_{O_2}(x,t)/c_{ref}$, $a_{H_2O_2}(x,t) = c_{H_2O_2}(x,t)/c_{ref}$. Time dependance and spatial profile of electric potential between Pt and adjacent ionomer $U_{Pt}(x,t)$ will be further explained in the next section. The size of Pt particles $r_{Pt} = r_{Pt}(x)$, affecting the limiting diffusion flux of species to Pt surface, can in general evolve with time due to degradation of catalyst layer and growth of Pt band in the membrane, but is assumed to be stationary in the proposed

model. The term $b_T = RT/F$ describes the temperature dependence, while the diffusion constants D_i for all species refer to their values in the ionomer.

To relate the reaction rates to the changes in species concentrations, we need to consider the spatial distribution of Pt surface on which the reaction can take place, and the volume in which the species can reside. We express these properties as volume specific Pt surface density

$$\lambda_{\mathrm{Pt}}(x) = \frac{4\pi r_{\mathrm{Pt}}(x)^2}{\epsilon_{\mathrm{ion}}(x) + \epsilon_0(x)\dfrac{H_i}{RT}} n_{\mathrm{Pt}}(x) \tag{18}$$

where $n_{\mathrm{Pt}}(x)$ is volumetric density of Pt particles and effective volume modification is the same as for the case of diffusion equations. The spatial distribution of $\lambda_{\mathrm{Pt}}(x)$ describes the differences in distribution of Pt catalyst throughout the entire MEA and thus allows the use of the same form of electrochemical reaction rates in all MEA components. The rates of concentration changes can therefore be calculated for entire MEA as

$$\left(\frac{\partial c_{\mathrm{H_2}}(x,t)}{\partial t}\right)_{\mathrm{EC}} = -\lambda_{\mathrm{Pt}}(x)\, j_{\mathrm{HOR}}(x,t) \tag{19}$$

$$\left(\frac{\partial c_{\mathrm{O_2}}(x,t)}{\partial t}\right)_{\mathrm{EC}} = -\lambda_{\mathrm{Pt}}(x)\left[j_{\mathrm{ORR2}}(x,t) + j_{\mathrm{ORR4}}(x,t)\right] \tag{20}$$

$$\left(\frac{\partial c_{\mathrm{H_2O_2}}(x,t)}{\partial t}\right)_{\mathrm{EC}} = \lambda_{\mathrm{Pt}}(x)\left[j_{\mathrm{ORR2}}(x,t) - j_{\mathrm{PRR}}(x,t)\right] \tag{21}$$

It should be noted that the model does not describe the dynamics of water and proton concentration in the MEA, which are assumed to be constant and uniformly distributed.

Electric charging of Pt surface

The spatial distribution of electric potential on catalyst particles $U_{\mathrm{Pt}}(x,t)$ is crucial for adequate modelling of hydrogen peroxide formation. As seen from reaction rate Eq. (16), the formation of hydrogen peroxide is suppressed in the electric potential range between 0.67 and 1.23 V, where water production via ORR4 Eq. (15) is dominant. ORR2 only becomes significant at potential below 0.67 V. Since cathode and anode are electrically connected to the external load of the fuel cell, their electric potential can be controlled and measured by electric current through the fuel cell, making it possible to estimate which EC reactions will take place. It is assumed that potential of the Pt band is determined by the rates of EC reactions on its surface, since particles inside the Pt band are not easily accessible. Therefore, potential of the Pt is in turn determined by local concentrations of species in the membrane. Reduction reactions, such as HOR, produce electrons, which are deposited on Pt particles and thus reduce the electric potential, while oxidation reactions consume electrons and consequently increase the potential. This process is modelled by equation [21]

$$\left(\frac{\partial U_{\mathrm{Pt}}(x,t)}{\partial t}\right)_{\mathrm{EC}} = \frac{F}{\zeta_{DL}}\left[-2j_{\mathrm{HOR}}(x,t) + 4j_{\mathrm{ORR4}}(x,t) + 2j_{\mathrm{ORR2}}(x,t) + 2j_{\mathrm{PRR}}(x,t)\right] \tag{22}$$

where $\zeta_{\mathrm{DL}} = C_{\mathrm{DL}}/S$ is a surface specific double layer capacitance of the Pt surface [22]. In cathode and anode catalyst layer, the potential is also affected by electric conduction through carbon support structure, which causes the spatial distribution of potential to equilibrate to a constant value throughout the catalyst layer. This process is modelled by diffusion-like equation [21]

$$\left(\frac{\partial U_{\mathrm{Pt}}(x,t)}{\partial t}\right)_{\mathrm{cond}} = -\frac{1}{4\pi r_{\mathrm{Pt}}(x)^2 n_{\mathrm{Pt}}(x)\zeta_{\mathrm{DL}}}\frac{\partial}{\partial x}\left(\sigma_{\mathrm{eff}}(x)\frac{\partial U_{\mathrm{Pt}}(x,t)}{\partial x}\right) \tag{23}$$

Volumetric capacitance of catalyst layer is calculated as a product of Pt surface capacitance and Pt surface density. Effective electric conductivity is determined from catalyst volumetric ratio $\varepsilon_{PtC}(x)$ and bulk carbon conductivity σ_C as $\sigma_{\mathrm{eff}}(x) = \sigma_C\,\varepsilon_{\mathrm{PtC}}(x)^{\alpha}$. It should be noted that since the catalyst volumetric ratio inside the membrane is zero, electric conduction only affects the potential in the catalyst layers.

Fenton reactions

The hydrogen peroxide produced in electrochemical reactions reacts with metal ions in a series of reactions, resulting in formation of radical species. This process is typically modelled as a set of Fenton reactions with iron ions [6,17], which can be simplified to a single reaction,

$$Fe^{2+/3+} + 2H_2O_2 \rightarrow Fe^{2+/3+} + HO^{\bullet} + HOO^{\bullet} + H_2O \tag{24}$$

Since we are only interested in the current model with spatial distribution of hydrogen peroxide formation, but not in further chemical membrane degradation processes [6,7], the Fenton-like consumption of peroxide is modelled by a simple equation

$$\left(\frac{\partial c_{\mathrm{H_2O_2}}(x,t)}{\partial t}\right)_{\mathrm{fent}} = -k_{\mathrm{fent}}c_{\mathrm{H_2O_2}}(x,t) \tag{25}$$

where k_{fent} is related to the effective reaction rate of Fenton reaction and to the concentration of relevant transition metal ions present in the ionomer, which are assumed to be uniformly dispersed through the MEA.

Boundary conditions

Boundary conditions for concentration profiles are applied at the boundary between cathode and gas diffusion layer (GDL) at $x = 0$, and between anode and GDL at $x = d_{\mathrm{MEA}}$. Hydrogen and oxygen boundary conditions are determined by diffusive flux of species through the gas diffusion layer (GDL) with effective diffusivity $\tilde{D}_{\mathrm{i,GDL}} = D_{\mathrm{i,GDL}}H_{\mathrm{i}}/RT$ expressed in terms of ionomer concentration.

$$\left(\tilde{D}_{\mathrm{O_2}}(x)\frac{\partial c_{\mathrm{O_2}}(x,t)}{\partial x}\right)_{x=0} = \frac{\tilde{D}_{\mathrm{O_2,GDL}}}{d_{\mathrm{GDL}}}\left[\frac{RT}{H_{O_2}}c_{\mathrm{O_2,ch}}(t) - c_{\mathrm{O_2}}(0,t)\right] \tag{26}$$

$$\left(\tilde{D}_{\mathrm{H_2}}(x)\frac{\partial c_{\mathrm{H_2}}(x,t)}{\partial x}\right)_{x=0} = -\frac{\tilde{D}_{\mathrm{H_2,GDL}}}{d_{\mathrm{GDL}}}c_{\mathrm{H_2}}(0,t) \tag{27}$$

$$\left(\tilde{D}_{\mathrm{H_2O_2}}(x)\frac{\partial c_{\mathrm{H_2O_2}}(x,t)}{\partial x}\right)_{x=0} = -\frac{\tilde{D}_{\mathrm{H_2O_2,GDL}}}{d_{\mathrm{GDL}}}c_{\mathrm{H_2O_2}}(0,t) \tag{28}$$

$$\left(\tilde{D}_{\mathrm{O_2}}(x)\frac{\partial c_{\mathrm{O_2}}(x,t)}{\partial x}\right)_{x=d_{\mathrm{MEA}}} = \frac{\tilde{D}_{\mathrm{O_2,GDL}}}{d_{\mathrm{GDL}}}c_{O_2}(d_{\mathrm{MEA}},t) \tag{29}$$

$$\left(\tilde{D}_{\mathrm{H_2}}(x)\frac{\partial c_{\mathrm{H_2}}(x,t)}{\partial x}\right)_{x=d_{\mathrm{MEA}}} = \frac{\tilde{D}_{\mathrm{H_2,GDL}}}{d_{\mathrm{GDL}}}\left[c_{\mathrm{H_2}}(d_{\mathrm{MEA}},t) - \frac{RT}{H_{\mathrm{H_2}}}c_{\mathrm{H_2,ch}}(t)\right] \tag{30}$$

$$\left(\tilde{D}_{\mathrm{H_2O_2}}(x)\frac{\partial c_{\mathrm{H_2O_2}}(x,t)}{\partial x}\right)_{x=d_{\mathrm{MEA}}} = \frac{\tilde{D}_{\mathrm{H_2O_2,GDL}}}{d_{\mathrm{GDL}}}c_{\mathrm{H_2O_2}}(d_{\mathrm{MEA}},t) \tag{31}$$

Hydrogen concentration in anode gas feed channel $c_{H_2,ch}(t)$ and oxygen in cathode gas feed channel is $c_{O_2,ch}(t)$. We assume that hydrogen concentration in cathode channel and oxygen concentration in anode channel is zero. For hydrogen peroxide we assume that concentration in both channels is zero [17].

Boundary conditions for electric potential are determined from electric current density j_{El} drawn from the fuel cell:

$$\left(\sigma_{\text{eff}}(x)\frac{\partial U_{\text{Pt}}(x,t)}{\partial x}\right)_{x=0} = -j_{\text{El}} \tag{32}$$

$$\left(\sigma_{\text{eff}}(x)\frac{\partial U_{\text{Pt}}(x,t)}{\partial x}\right)_{x=d_{\text{MEA}}} = -j_{\text{El}} \tag{33}$$

Note that negative sign in boundary condition at $x = 0$ describes electric current flowing out of the cathode, while at $x = d_{\text{MEA}}$ negative sign describes current flowing into the anode.

Experimental data

The model was tested and verified on the experimental data, obtained from the paper by Ohma *et al.* [10]. In their experiment, the durability of fuel cell membrane was related to the deposition of catalyst in the Pt band. The degradation experiment was performed for 48 hours in open-circuit voltage (OCV) operation fuel cell at T = 90 °C with pure hydrogen and oxygen at ambient pressure as a fuel. As indication of membrane degradation, the Raman spectrum of ionomer was measured at several locations across the aged membrane thickness. Additionally, the size and density of Pt particles in the membrane were measured using transmission electron microscopy.

The aim of model verification is to determine whether the position of hydrogen peroxide production, determined by the proposed model, overlaps with the location of maximal membrane degradation, measured in the experiment. To reproduce the experimental conditions, the following model parameters need to be determined: spatial distribution of Pt particle size $r_{\text{Pt}}(x)$, Pt particle density $n_{\text{Pt}}(x)$, void volume fraction $\varepsilon_0(x)$, ionomer volume fraction $\varepsilon_{\text{ion}}(x)$, temperature T and boundary conditions.

The thickness of cathode and anode, used in experiment, are $d_{\text{cat}} = d_{\text{cat}}$ = 10 µm. The membrane thickness changed from initial 50 to 33 µm after degradation. In the model, we used the latter value for easier comparison with the Raman measurement, d_{mem} = 33 µm. Particle size and density distribution were determined separately for cathode ($0 < x < d_{\text{cat}}$), membrane ($d_{\text{cat}} < x < d_{\text{cat}} + d_{\text{mem}}$) and anode ($d_{\text{cat}} + d_{\text{mem}} < x < d_{\text{MEA}}$).

For cathode and anode catalyst layer, $r_{\text{Pt}}(x)$ and $n_{\text{Pt}}(x)$ were assumed to be constant and were determined from the data on catalyst properties, namely Pt loading (Pt_{Load})= 0.35 mg/cm^2 and electrochemical surface area ESA = 80 m^2/g (deduced from the type of catalyst, TEC10E50E, TKK, [23]). Particle size and density are calculated as [24]:

$$r_{\text{Pt}} = \frac{3}{1000\rho_{\text{Pt}}\text{ESA}} = 1.78 \text{ nm} \tag{34}$$

$$n_{Pt} = \frac{3}{4}\frac{\text{Pt}_{\text{Load}}}{r_{\text{Pt}}^3\rho_{\text{Pt}}} = 7.0\times10^{23} \text{ m}^{-3} \tag{35}$$

The paper [10] provides the detailed measurement of properties of Pt particles in the membrane, such as size distribution and spatial distribution of particles above certain threshold. Based on this data, the spatial distribution of Pt band particle size $r_{\text{Pt}}(x)$ and density $n_{\text{Pt}}(x)$ in the membrane, $d_{\text{cat}} < x < d_{\text{cat}} + d_{\text{mem}}$ was constructed. According to numerical study of Pt band growth in the membrane by Burlatsky *et al.*, the volumetric density of particles in the membrane is determined by

agglomeration dynamics during Pt band formation and is homogeneous throughout the membrane [11]. Based on estimated Pt ion flux to the membrane from [10], constant distribution $n_{Pt}(x)$ = 2.08 × 10^{18} m^{-3} was assumed. Size distribution $r_{Pt}(x)$ was reconstructed from measured distribution of particles larger than 25 nm and was described in the model as a normal distribution

$$r_{Pt}(x) = r_{Pt,max} e^{-\frac{(x-\bar{x}_{band})^2}{2(\sigma_{band})^2}} \quad (36)$$

with mean value $\bar{x}_{band} = d_{cat} + 0.4\, d_{mem}$, standard deviation $\sigma_{band} = 0.096\, d_{mem}$ and maximal size of particles $r_{Pt,max}$ = 12.3 nm. Spatial distribution of particle size and density for entire MEA is plotted in Figure 2.

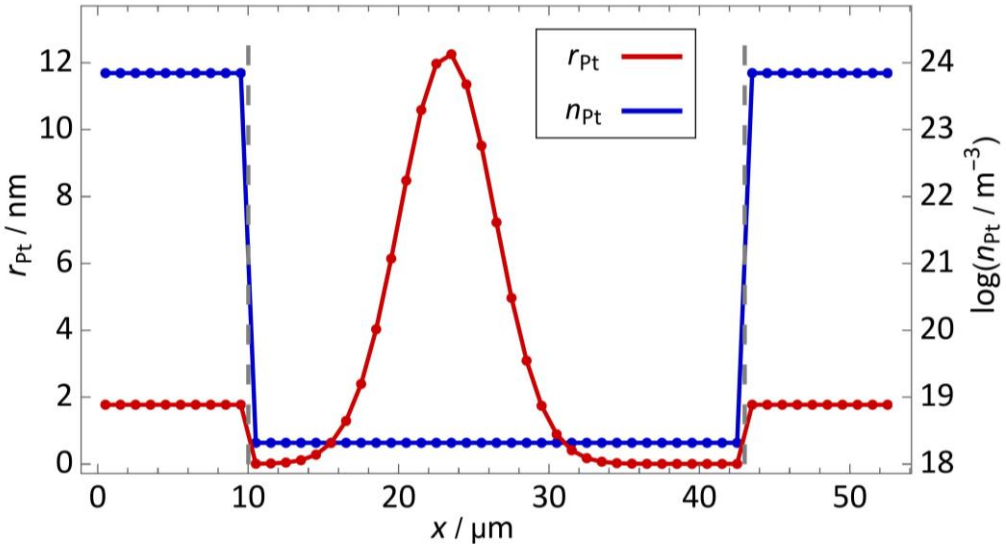

Figure 2. *Spatial distribution of particle size* $r_{Pt}(x)$ *and density* $n_{Pt}(x)$ *through the MEA, used in the model (constructed based on data from [10])*

Ionomer volume fraction in the membrane was set to ε_{ion} = 1, while in the catalyst layers, volumetric ratios were calculated from the data, provided in [10]. Catalyst volumetric ratio was determined from Pt loading and Pt/C ratio (50:50), ε_{PtC} = 0.191, and ionomer volumetric ratio was determined from Nafion to carbon mass ratio (m_{naf}/m_C = 0.9), ε_{ion} = 0.199.

Since pure oxygen and hydrogen at ambient pressure and T = 90 °C were used in the experiment, their respective concentrations in the gas feed channels, used as boundary conditions, were calculated as $c_{O_2,ch}(t) = c_{O_2,ch}(t) = p/RT$ = 33.6 mol m^{-3}. Boundary condition for electric potential is determined from OCV operation to be j_{El} = 0.

Diffusion constant in GDL was assumed to be proportional to void diffusion constant. GDL thickness, used in experiment (20BC, SGL Carbon), was d_{GDL} = 235 µm and diffusivity was calculated from bulk diffusivity as $D_{i,GDL} = Q\, D_{i,0}$ with Q = 0.139 [25].

Material parameters used in diffusion model were obtained from two papers by Wong *et. al* [16,17] and are listed in Table 1.

Table 1. *Diffusion model parameters*

Species	D / m^2 s^{-1}	Reference	Species	H / Pa m^3 mol^{-1}	Reference
O_2, gas phase	1.98×10^{-5}	[17]	O_2	$4.718\times10^4\, e^{-666/T}$	[16] fit
H_2, gas phase	11.50×10^{-5}	[17]	H_2	$2.584\times10^4\, e^{170/T}$	[16]
H_2O_2, gas phase	1.88×10^{-5}	[17]	H_2O_2	$6.830\times10^7\, e^{-7379/T}$	[16]
O_2, ionomer phase	0.96×10^{-10}	[17]			
H_2, ionomer phase	2.08×10^{-10}	[17]			
H_2O_2, ionomer phase	1.50×10^{-10}	[17]			

As explained in [26], the position of Pt band in the membrane is determined by the values of diffusion and Henry constants of oxygen and hydrogen. To ensure that values of this parameters are consistent with the measured position of Pt band, Henry constant of oxygen H_{O_2} was reduced by a factor of 3.5 compared to the value, given in [16], designated by "fit" in Table 1. This could be justified by effects of humidity on H_{O_2} [27], which are not taken into account by the expression, provided in [16].

Material parameters used in electrochemical reaction model were obtained from [17] and are listed in Table 2. Specific surface capacity of Pt particles ζ_{DL} = 40 μF cm^{-2} was obtained from [22].

Table 2. *Electrochemical reaction* parameters

Reaction	k / A m^{-2}	Reference	Reaction	α	Reference
HOR	10^5	[17]	HOR	0.50	[17]
ORR2	40	[17]	ORR2	0.50	[17]
ORR4	50	[17]	ORR4	0.50	[17]
PRR	10^{-13}	[15]	PRR	0.32	[17]

The value of reaction rate constant for Fenton reactions was calculated according to [6] as

$$k_{fent} = k_0 c_{Fe^{2+/3+}} \quad (37)$$

with $k_0 = A\, e^{-Ea/RT}$ = 845 M^{-1} s^{-1} at T = 363 K. Iron ions concentration was calibrated to obtain best fit between measured degradation profile and modelled peroxide concentration, resulting in value $c_{Fe^{2+/3+}}$ = 600 ppm, which is consistent with the values, reported in [6].

Numerical simulations

With the model parameters set up based on experimental data, three numerical simulations were performed using the model implemented in Python programming language. Differential equation Eq. (1)-(4) governing the equations were solved on computational grid with 10 control volumes in cathode and anode catalyst layer and 33 control volumes in the membrane (Δx = 1 μm) using Scipy solver "solve_ivp" using "BDF" integration method [28].

In Simulation A, the model simulated operation of the fuel cell, described in section Experimental data, with already established and stationary Pt band. Since proposed model was not aimed to focus on chemical membrane degradation (this is covered in our previous publications [6,7]), but on the spatial distribution of hydrogen peroxide formation, the simulation time of 600 s was sufficient to achieve stationary MEA conditions and extract the results, which are compared to the experimentally measured spatial distribution of chemical membrane degradation.

After validation, the capabilities of the model were tested in two further simulations in fuel cell operating regimes where peroxide formation is expected to occur in either cathode or anode catalyst layer. As explained in Introduction, anode peroxide formation is expected from oxygen diffusing through the membrane to the anode, so Simulation B was performed with fuel cell in OCV operation with no Pt band present in the membrane ($r_{Pt}(x)$ = 0). Cathode peroxide formation is expected at low electric potential on cathode, which is a result of high electric current, so Simulation C was performed at sufficiently high electric current density to reproduce this behaviour: j_{El} = 10 A cm^{-2}.

Results and discussion

Simulation A

With the first simulation, we want to verify that the model predicts the formation of hydrogen peroxide in the membrane, consistent with the observed membrane degradation. The spatial distribution of species concentrations $c_{O_2}(x)$, $c_{H_2}(x)$, $c_{H_2O_2}(x)$ and electric potential $U_{Pt}(x)$ in stationary conditions are shown in Figure 3.

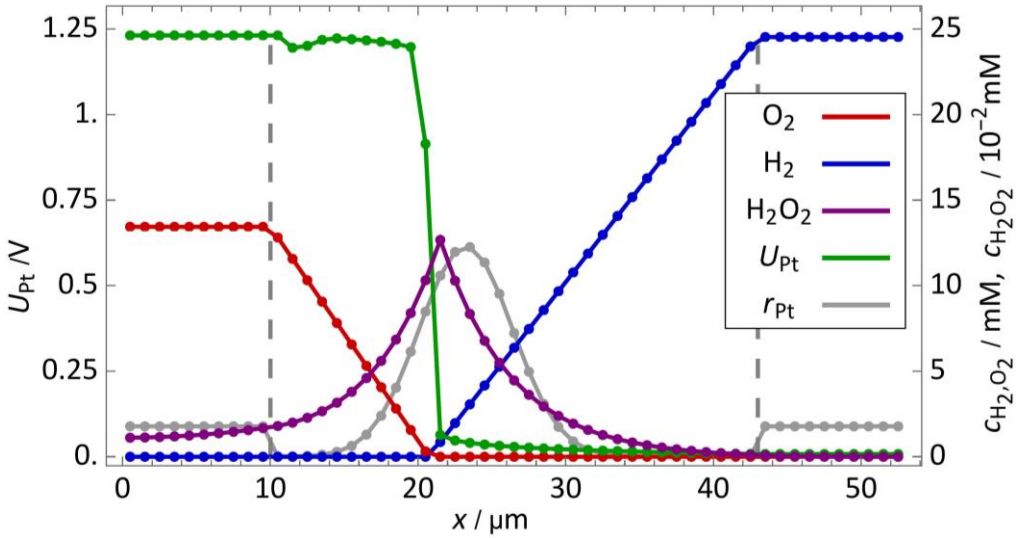

Figure 3. *Spatial distribution of oxygen* (*red*)*, hydrogen* (*blue*)*, hydrogen peroxide* (*purple*) *and electric potential* (*green*) *in OCV fuel cell operation with aged membrane* (*Simulation A*)*. Hydrogen peroxide forms mostly on Pt band as a result of oxygen reduction on Pt particles with low local electric potential*

Due to high gas diffusivity in porous catalyst compared to the membrane, the concentrations of oxygen and hydrogen (red and blue line in Figure 2, respectively) are uniform in the catalyst layer. Different concentrations of reactants despite the same concentrations in channels are a result of different Henry constants. Concentrations then fall linearly in the membrane towards zero, indicating a flux of reactants towards the Pt band, where oxygen and hydrogen are consumed in reactions ORR2, ORR4 and HOR. The electric potential $U_{Pt}(x)$ (green line in Figure 2) is determined by the rates of these reactions, Eq. (22). Left of the Pt band, high concentration of oxygen results in ORR reactions being more prominent than HOR, leading to consumption of electrons and thus increasing the local electric potential to a value close to ORR4 equilibrium 1.23 V, shifted by the concentration-dependent Nernst term [29]. Right of the Pt band, high hydrogen concentration promotes HOR reaction, resulting in deposition of electrons on Pt particles, thus lowering their potential close to 0 V.

At the location of oxygen-hydrogen mixing, the potential sharply transitions from one value to the other. This provides the conditions with sufficiently low electric potential ($U_{Pt} < 0.67$ V) and sufficiently high oxygen concentration which result in the formation of hydrogen peroxide (purple line in Figure 3). Hydrogen peroxide thus produced diffuses into the rest of the MEA, where it is consumed by peroxide reduction reaction and Fenton reaction. The concentration of hydrogen peroxide at its peak is about $c_{H_2O_2,max} \approx 0.12$ mM, which is consistent with the data, reported in [6].

Since Fenton reaction rate is proportional to the $c_{H_2O_2}(x)$ and since the reactions between radical species and the membrane structure are fast [6], we argue that the degradation rate of the membrane is proportional to the hydrogen peroxide concentration [6]. To verify this claim, we plot in Figure 4 the spatial profile of hydrogen peroxide concentration and spatial distribution of specific chemical bonds

in the membrane, measured by Raman spectroscopy [10]. The changes in relative intensity between SO bonds (red line in Figure 3) and CO bonds (orange line in Figure 3), found in sidechains of Nafion structure, compared to CF bonds, indicate the presence of chemical degradation phenomena. The spatial distribution of hydrogen peroxide concentration, predicted by the proposed model, coincides well with the observed degradation, confirming the validity of the modelling approach.

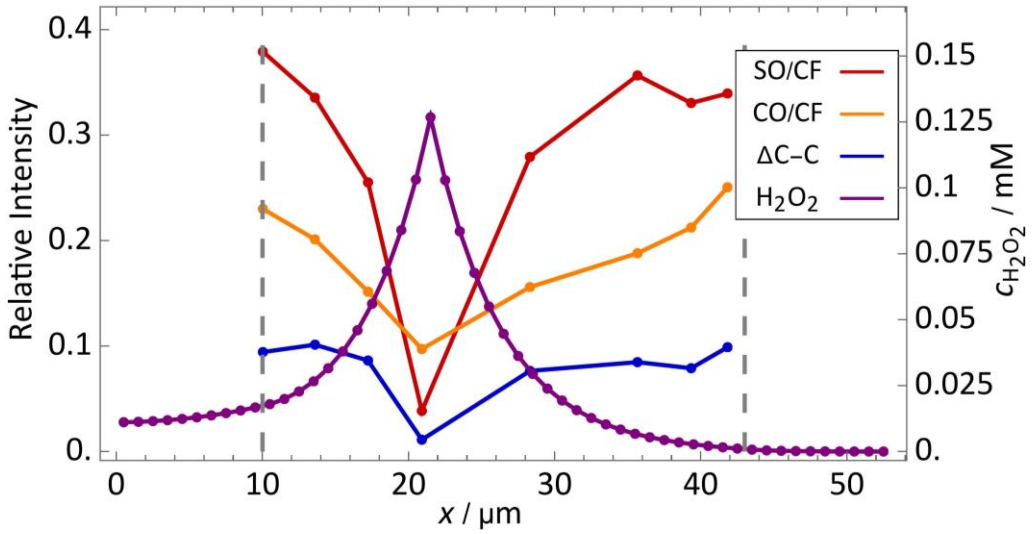

Figure 4. *Spatial distribution of hydrogen peroxide (purple), compared to the spatial distribution of specific membrane chemical bonds measured by Raman spectroscopy [10]*

Simulation B

As demonstrated in Simulation A, the reactions of oxygen and hydrogen on Pt band particles play a crucial role in determining the rate and location of hydrogen peroxide formation. With the second simulation we want to explore the process of hydrogen peroxide formation in fresh MEA, where no Pt band particles are present in the membrane, in OCV conditions. The results of simulation for stationary conditions are shown in Figure 5.

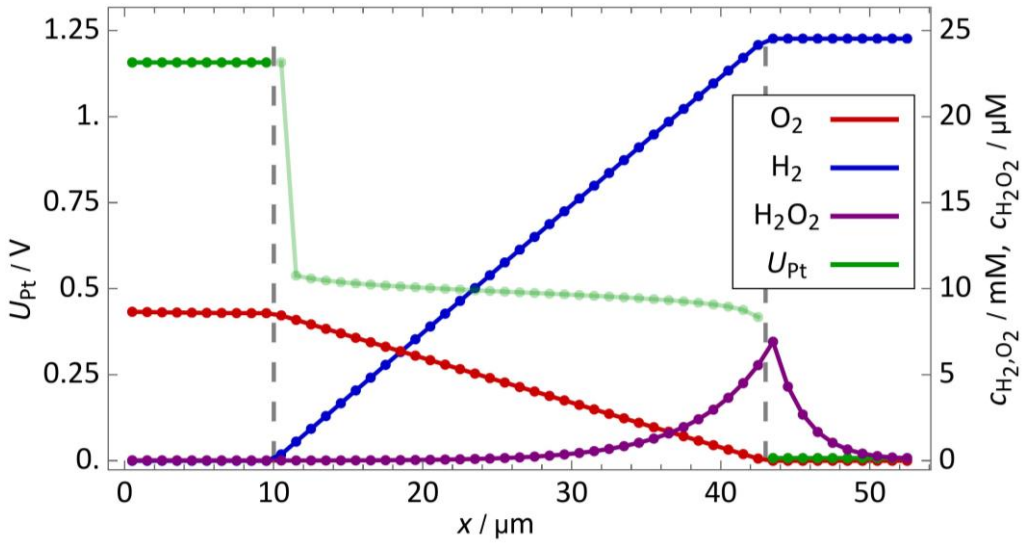

Figure 5. *Spatial distribution of oxygen (red), hydrogen (blue), hydrogen peroxide (purple) and electric potential (green) at OCV fuel cell operation with fresh membrane (no Pt band, Simulation B). Hydrogen peroxide mostly forms at the anode from crossover oxygen flux through the membrane*

Similarly to the results of Simulation A, oxygen and hydrogen concentrations are constant in catalyst layers and change linearly through the membrane, but now gases diffuse not to the position of

Pt band, but to their respective counter-electrode, where they immediately react due to large difference between equilibrium and local electric potential (green). In case of oxygen diffusing to the anode, this results in reaction at electric potential $U_{Pt} \approx 0$ V < U_{ORR2}, which leads to the formation of hydrogen peroxide. Its concentration is somewhat lower compared to the case of Pt band formation ($c_{H_2O_2,max} \approx 7$ µM), which can be explained by slower diffusion of oxygen to the anode due to longer diffusion path. Note that since no Pt particles are present in the membrane, the values of electric potential in this region (light green) are a residual of the model and play no role in electrochemical reactions.

Simulation C

In the last simulation, we want to explore the conditions in which the peroxide formation would occur at the cathode catalyst layer. As explained in Introduction, this would require sufficiently low electric potential at the cathode, which is in a fuel cell a result of high electric current density. In Simulation C we again model a fresh membrane with no Pt band and with external electric current density $j_{El} = 10$ A/m^2. Note that this value is unrealistically high for an actual fuel cell, so the results should be taken only as a demonstration of the model capabilities with no direct quantitative value. The spatial distributions, resulting from Simulation C, are shown in Figure 6.

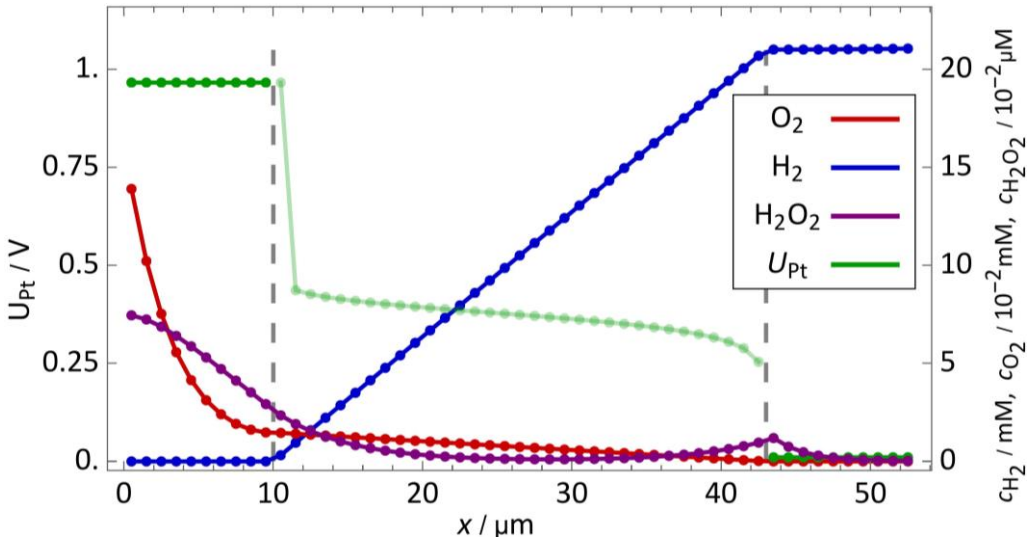

Figure 6. *Spatial distribution of oxygen* (*red*)*, hydrogen* (*blue*)*, hydrogen peroxide* (*purple*) *and electric potential* (*green*) *in fuel cell with fresh membrane* (*no Pt band*) *operating at high electric current density* (*Simulation C*)*. Hydrogen peroxide forms on both cathode and anode side, but with small overall concentration*

At the specified high current density, most of the oxygen is consumed in the cathode catalyst layer (note that oxygen and hydrogen concentration in Figure 6 are not plotted in the same scale), resulting in the lowering of cathode electric potential. The hydrogen peroxide (purple) formation now takes place both in cathode and anode catalyst layer but is more prominent in cathode due to higher concentration of oxygen. Note, however, that the overall hydrogen peroxide concentration ($c_{H_2O_2,max} \approx 7 \times 10^{-2}$ µM) is much lower compared to Simulation A or Simulation B.

The results of Simulations A, B and C highlight the importance of both fuel cell operating conditions as well as its state of health in identifying the location and rate of hydrogen peroxide production in fuel cell MEA. Due to low electric potential, the anode is more prone to hydrogen peroxide formation, under the condition that oxygen is present in the anode, which might not be the case if the Pt band is formed in the membrane. Cathode, despite its abundance of oxygen, does

not seem to be an important source of hydrogen peroxide at moderate or normal current densities since high electric potential strongly promotes the reaction of oxygen to water (ORR4).

Conclusion

In the paper we present a one-dimensional model of coupled physical processes, contributing to the formation of hydrogen peroxide in the LT-PEMFC membrane-electrode assembly. The model describes spatial distribution of oxygen, hydrogen, and hydrogen peroxide concentration as well as spatial distribution of local electric potential between catalyst particles and adjacent ionomer. The diffusion of chemical species is governed by a unified set of equations, considering the material composition and porosity of different MEA components. Consumption and production of species in electrochemical reactions across MEA is described by a unified description of reaction rates in terms of contributions of local electric potential, available catalyst surface and diffusion limitations due to finite size of catalyst particles. Electric potential of active catalyst particles is calculated by considering both external electric currents through to the catalyst layer and charging of double layer on particle surface due to electrochemical reactions on catalyst particles.

The validity of the model was confirmed by successfully reproducing the spatial distribution of hydrogen peroxide concentration in OCV degradation experiment, which coincides well with experimentally determined spatial distribution of membrane degradation, measured by Raman spectroscopy [10]. The results of this simulation reveal a rich interplay between intertwined physical processes incorporated in the presented model. Diffusion of oxygen and hydrogen through the membrane and their electrochemical consumption at Pt band results in non-trivial spatial distribution of local electric potential, which transitions from high value of $U_{Pt} \approx 1.23$ V in oxygen rich environment to low value of $U_{Pt} \approx 0.0$ V in hydrogen rich environment. The transitioning area inside the Pt band thus features appropriate electric potential and sufficient oxygen concentration, suitable for hydrogen peroxide formation. Further numerical simulations of fresh MEA without Pt band indicate that both position as well as rate of hydrogen peroxide formation depends strongly on fuel cell operating conditions via coupled dynamics of reactants spatial distribution and resulting electric potential on catalyst particles.

Due to its strong explanatory power, the proposed model elucidates causal relations of peroxide formation phenomena and comparison of formation rates at different locations at different fuel cell operating conditions. The model, therefore, represents a solid background for further theoretical exploration of dynamics of hydrogen peroxide formation in LT-PEMFC systems. Since the results of the model can easily be related to the experimentally observed phenomena via Raman spectroscopy analysis of the membrane, the model also serves as useful tool in designing new experiments, exploring the detailed mechanisms of hydrogen peroxide formation, which might have not yet been sufficiently elaborated. After availability of more detailed experimental data and extensive model validation as well as calibration of its parameters, the proposed model can be characterized as a powerful toll for designing advanced fuel cell operation strategies and fuel cell designs, aimed at minimizing the degradation processes in the LT-PEMFC, improving its performance, and increasing its lifetime.

***Acknowledgements**: This work has been partly conducted within the MORELife project and has received funding from the Fuel Cells and Hydrogen 2 Joint Undertaking (JU) under grant agreement No 101007170. The JU receives support from the European Union's Horizon 2020 research and innovation programme and Hydrogen Europe and Hydrogen Europe Research. The research is part of project "ARRS-CEA NC-0025"**. The research is partially funded by the Slovenian Research Agency (research core funding no. P2-0401).*

References

[1] S. M. J. Zaidi, M. A. Rauf, *Fuel Cell Fundamentals*, in *Polymer Membranes for Fuel Cells*, S. M. Javaid Zaidi, T. Matsuura, Eds., Springer US, Boston, USA, 2008, p. 1-6. https://doi.org/10.1007/978-0-387-73532-0_1

[2] T. Jahnke, G. Futter, A. Latz, T. Malkow, G. Papakonstantinou, G. Tsotridis, P. Schott, M. Gérard, M. Quinaud, M. Quiroga, A. A. Franco, K. Malek, F. Calle-Vallejo, R. Ferreira de Morais, T. Kerber, P. Sautet, D. Loffreda, S. Strahl, M. Serra, P. Polverino, C. Pianese, M. Mayur, W. G. Bessler, C. Kompis, Performance and degradation of Proton Exchange Membrane Fuel Cells: State of the art in modeling from atomistic to system scale, *Journal of Power Sources* **304** (2016) 207-233. https://doi.org/10.1016/j.jpowsour.2015.11.041

[3] A. Kregar, M. Gatalo, N. Maselj, N. Hodnik, T. Katrašnik, Temperature dependent model of carbon supported platinum fuel cell catalyst degradation, *Journal of Power Sources* **514** (2021) 230542. https://doi.org/10.1016/j.jpowsour.2021.230542

[4] A. Kregar, G. Tavčar, A. Kravos, T. Katrašnik, *EFCF 2019 - Low-Temperature Fuel Cells, Electrolysers and H_2 Processing* ,Fundamentals and Engineering Design *Predictive model for performance and platinum degradation simulation of high temperature PEM fuel cells in transient operating conditions,* Lucerne, Switzerland, 2019, p. 1817-1822. https://past.efcf.com/index.php-id=proceedings_isbn.html

[5] A. Kregar, A. Kravos, T. Katrašnik, Methodology for Evaluation of Contributions of Ostwald Ripening and Particle Agglomeration to Growth of Catalyst Particles in PEM Fuel Cells, *Fuel Cells* **20** (2020) 487-498. https://doi.org/10.1002/fuce.201900208

[6] P. Frühwirt, A. Kregar, J.T. Törring, T. Katrašnik, G. Gescheidt, Holistic approach to chemical degradation of Nafion membranes in fuel cells: modelling and predictions, *Physical Chemistry Chemical Physics* **22** (2020) 5647-5666. https://doi.org/10.1039/C9CP04986J

[7] A. Kregar, P. Frühwirt, D. Ritzberger, S. Jakubek, T. Katrašnik, G. Gescheidt, Sensitivity based order reduction of a chemical membrane degradation model for low-temperature proton exchange membrane fuel cells, *Energies* **13(21)** (2020) 5611. https://doi.org/10.3390/en13215611.

[8] V. A. Sethuraman, J. W. Weidner, A. T. Haug, M. Pemberton, L. V. Protsailo, Importance of catalyst stability vis-à-vis hydrogen peroxide formation rates in PEM fuel cell electrodes, *Electrochimica Acta* **54** (2009) 5571-5582. https://doi.org/10.1016/j.electacta.2009.04.062

[9] V. A. Sethuraman, J. W. Weidner, A. T. Haug, S. Motupally, L. V. Protsailo, Hydrogen Peroxide Formation Rates in a PEMFC Anode and Cathode, *Journal of The Electrochemical Society* **155** (2008) B50. https://doi.org/10.1149/1.2801980

[10] A. Ohma, S. Yamamoto, K. Shinohara, Membrane degradation mechanism during open-circuit voltage hold test, *Journal of Power Sources* **182** (2008) 39-47. https://doi.org/10.1016/j.jpowsour.2008.03.078

[11] S. F. Burlatsky, M. Gummalla, V. V. Atrazhev, D. V. Dmitriev, N.Y. Kuzminyh, N. S. Erikhman, The Dynamics of Platinum Precipitation in an Ion Exchange Membrane, *Journal of The Electrochemical Society* **158** (2011) B322. https://doi.org/10.1149/1.3532956

[12] M. Holber, P. Johansson, P. Jacobsson, Raman spectroscopy of an aged low temperature polymer electrolyte fuel cell membrane, *Fuel Cells* **11** (2011) 459-464. https://doi.org/10.1002/fuce.201100006

[13] H. Ericson, T. Kallio, T. Lehtinen, B. Mattsson, G. Sundholm, F. Sundholm, P. Jacobsson, Confocal Raman Spectroscopic Investigations of Fuel Cell Tested Sulfonated Styrene Grafted Poly(vinylidene fluoride) Membranes, *Journal of The Electrochemical Society* **149** (2002) A206. https://doi.org/10.1149/1.1431964

[14] V. A. Sethuraman, J. W. Weidner, A. T. Haug, S. Motupally, L. V. Protsailo, Hydrogen Peroxide Formation Rates in a PEMFC Anode and Cathode, *Journal of The Electrochemical Society* **155** (2008) B50. https://doi.org/10.1149/1.2801980
[15] C. Chen, T. F. Fuller, Modeling of H_2O_2 formation in PEMFCs, *Electrochimica Acta* **54** (2009) 3984-3995. https://doi.org/10.1016/j.electacta.2009.02.021
[16] K. H. Wong, E. Kjeang, Macroscopic In-Situ Modeling of Chemical Membrane Degradation in Polymer Electrolyte Fuel Cells, *Journal of The Electrochemical Society* **161** (2014) F823-F832. https://doi.org/10.1149/2.0031409jes
[17] K .H. Wong, E. Kjeang, Mitigation of Chemical Membrane Degradation in Fuel Cells: Understanding the Effect of Cell Voltage and Iron Ion Redox Cycle, *ChemSusChem* **8** (2015) 1072-1082 https://doi.org/10.1002/cssc.201402957
[18] R. Singh, P.C. Sui, K. H. Wong, E. Kjeang, S. Knights, N. Djilali, Modeling the Effect of Chemical Membrane Degradation on PEMFC Performance, *Journal of The Electrochemical Society* **165** (2018) F3328-F3336. https://doi.org/10.1149/2.0351806jes
[19] G. A. Futter, A. Latz, T. Jahnke, Physical modeling of chemical membrane degradation in polymer electrolyte membrane fuel cells: Influence of pressure, relative humidity and cell voltage, *Journal of Power Sources* **410–411** (2019) 78-90. https://doi.org/10.1016/j.jpowsour.2018.10.085
[20] B. Tjaden, D.J.L. Brett, P.R. Shearing, Tortuosity in electrochemical devices: a review of calculation approaches, *International Materials Reviews* **63** (2018) 47-67. https://doi.org/10.1080/09506608.2016.1249995
[21] M. Eikerling, A. Kornyshev, Electrochemical impedance of the cathode catalyst layer in polymer electrolyte fuel cells, *Journal of Electroanalytical Chemistry* **475** (1999) 107-123. https://doi.org/10.1016/S0022-0728(99)00335-6
[22] W. G. Pell, A. Zolfaghari, B. E. Conway, Capacitance of the double-layer at polycrystalline Pt electrodes bearing a surface-oxide film, *Journal of Electroanalytical Chemistry* **532** (2002) 13-23. https://doi.org/10.1016/S0022-0728(02)00676-9
[23] Y. Garsany, J. Ge, J. St-Pierre, R. Rocheleau, K. E. Swider-Lyons, Analytical Procedure for Accurate Comparison of Rotating Disk Electrode Results for the Oxygen Reduction Activity of Pt/C, *Journal of The Electrochemical Society* **161** (2014) F628-F640. https://doi.org/10.1149/2.036405jes
[24] P. J. Ferreira, G. J. la O', Y. Shao-Horn, D. Morgan, R. Makharia, S. Kocha, H. A. Gasteiger, Instability of Pt⁄C Electrocatalysts in Proton Exchange Membrane Fuel Cells, *Journal of The Electrochemical Society* **152** (2005) A2256. https://doi.org/10.1149/1.2050347
[25] C. Chan, N. Zamel, X. Li, J. Shen, Experimental measurement of effective diffusion coefficient of gas diffusion layer/microporous layer in PEM fuel cells, *Electrochimica Acta* **65** (2012) 13-21. https://doi.org/10.1016/j.electacta.2011.12.110
[26] W. Bi, G. E. Gray, T. F. Fuller, PEM Fuel Cell Pt⁄C Dissolution and Deposition in Nafion Electrolyte, *Electrochemical Solid-State Letters* **10** (2007) B101. https://doi.org/10.1149/1.2712796
[27] R. F. Mann, J. C. Amphlett, B. A. Peppley, C. P. Thurgood, Henry's Law and the solubilities of reactant gases in the modelling of PEM fuel cells, *Journal of Power Sources* **161** (2006) 768-774. https://doi.org/10.1016/j.jpowsour.2006.05.054
[28] P. Virtanen, R. Gommers, T. E. Oliphant, M. Haberland, T. Reddy, D. Cournapeau, E. Burovski, P. Peterson, W. Weckesser, J. Bright, S. J. van der Walt, M. Brett, J. Wilson, K. J. Millman, N. Mayorov, A. R. J. Nelson, E. Jones, R. Kern, E. Larson, C. J. Carey, İ. Polat, Y. Feng, E. W. Moore, J. VanderPlas, D. Laxalde, J. Perktold, R. Cimrman, I. Henriksen, E. A. Quintero, C. R. Harris, A. M. Archibald, A. H. Ribeiro, F. Pedregosa, P. van Mulbregt, A. Vijaykumar, A. Pietro Bardelli, A. Rothberg, A. Hilboll, A. Kloeckner, A. Scopatz, A. Lee, A.

Rokem, C. N. Woods, C. Fulton, C. Masson, C. Häggström, C. Fitzgerald, D. A. Nicholson, D. R. Hagen, D. V. Pasechnik, E. Olivetti, E. Martin, E. Wieser, F. Silva, F. Lenders, F. Wilhelm, G. Young, G.A. Price, G.-L. Ingold, G. E. Allen, G. R. Lee, H. Audren, I. Probst, J. P. Dietrich, J. Silterra, J. T. Webber, J. Slavič, J. Nothman, J. Buchner, J. Kulick, J. L. Schönberger, J. V. de Miranda Cardoso, J. Reimer, J. Harrington, J. L. C. Rodríguez, J. Nunez-Iglesias, J. Kuczynski, K. Tritz, M. Thoma, M. Newville, M. Kümmerer, M. Bolingbroke, M. Tartre, M. Pak, N. J. Smith, N. Nowaczyk, N. Shebanov, O. Pavlyk, P. A. Brodtkorb, P. Lee, R. T. McGibbon, R. Feldbauer, S. Lewis, S. Tygier, S. Sievert, S. Vigna, S. Peterson, S. More, T. Pudlik, T. Oshima, T. J. Pingel, T. P. Robitaille, T. Spura, T.R. Jones, T. Cera, T. Leslie, T. Zito, T. Krauss, U. Upadhyay, Y. O. Halchenko, Y. Vázquez-Baeza, SciPy 1.0: fundamental algorithms for scientific computing in Python, *Nature Methods* **17** (2020) 261-272 https://doi.org/10.1038/s41592-019-0686-2

[29] A.-S. Feiner, A.J. McEvoy, The Nernst Equation, *Journal of Chemical Education* **71** (1994) 493. https://doi.org/10.1021/ed071p493